Research article

SURFACE and INTERFACE ANALYSIS

Received: 27 July 2012 Revised: 9 January 2013 Accepted: 9 January 2013 Published online in Wiley Online Library: 7 February 2013

(wileyonlinelibrary.com) DOI 10.1002/sia.5228

Ab-Initio calculations of the CO adsorption and dissociation on substitutional Fe–Cu surface alloys relevant to Fischer–Tropsch Synthesis: *bcc*-(Cu)Fe(100) and *fcc*-(Fe)Cu(100)

MohammadReza Elahifard,[a*] Elham Fazeli,[b] Azadeh Joshani[c] and MohammadReza Gholami[d]

Direct CO dissociation is seen the main path of the first step in the Fischer–Tropsch Synthesis (FTS) on the reactive iron surfaces. Cu/Fe alloy film is addressed with various applications over face-centered-cubic (*fcc*)-Cu and body-centered-cubic (*bcc*)-Fe in the FTS, i.e. preventing iron carbide formation (through direct CO dissociation) by moderating the surface reactivity and facilitating the reduction of iron surfaces, respectively. In this study by density functional theory, the stable configurations of CO molecule on various Cu/Fe alloys over *fcc*-Cu(100) and *bcc*-Fe(100) surfaces with different CO coverage (25% and 50%) have been evaluated. Our results showed that the ensemble effect plays a fundamental role to CO adsorption energy on the surface alloys over *bcc*-Fe(100); on the other hand, the ligand effect determines the CO stability on the *fcc*-Cu(100) surface alloys. CO dissociation barrier was also calculated on the surface alloys that showed although the CO dissociation process is thermodynamically possible on the more reactive surface alloys, but according to their high barrier, CO dissociation does not occur directly on these surfaces. Copyright © 2013 John Wiley & Sons, Ltd.

Keywords: co dissociation; Fischer–Tropsch synthesis; alloy film; density functional theory; ensemble effect; ligand effect

Introduction

The interaction of CO with transition and noble metals and their alloys conveys key mechanistic clues for understanding the fundamental steps of the reactions taking place in commercial catalysis, including both the hydrocarbon formation and the methanol reforming processes.[1–3] CO chemisorption on metal alloy surfaces has unique properties different from those of the corresponding elemental metals.[4–6] Groβ [4,7] provides evidence, based on first-principles calculations, of the *ensemble* and *ligand effects* being responsible for new properties of bimetallic catalysts. The former describes the minimum size of the adsorption complex with the required active sites for reactions to take place, and it may change dramatically after alloy formation; the latter implies the electronic structure of the system. Both ensemble and ligand effects are sensitive to the geometry of the catalyst support.[7] The d-band model,[8] which addresses the linear relationship between the shift of the d-band center and the changes in adsorption energy, could successfully explain surface alloy site activity on the basis of the d-band width. Narrow/broad d-bands shifted up/down in energy cause stronger/weaker interaction with the 2Π orbital of the adsorbed CO, and hence the model could shed light on the strength of chemisorption bond.[9]

Industrial catalysts based on Fe and its alloys are recently the subject of fundamental investigation in relation to Fischer–Tropsch synthesis (FTS).[10,11] Too high activity (higher CO adsorption energy and lower CO dissociation barrier) of the elemental metal gives rise to iron carbide formation under FTS conditions, and this is considered a possible deactivation avenue for FTS Fe catalysts.[12,13] Deposited iron atoms on the copper surfaces have been suggested as the optimal means of preventing iron carbide formation.[14] On the other hand, a role has been identified for copper as a promoter of iron surfaces that facilitates its reduction and shifts the hydrocarbon product distribution to higher molecular weight.[15] Hence, Cu/Fe alloy film is addressed with different application over face-centered-cubic (*fcc*)-Cu and body-centered-cubic (*bcc*)-Fe in the FTS. Most studies so far have focused on thin iron layers deposited on the surface of *fcc*-Cu.[16–18] Furthermore, non-equilibrium methods using Pb as a surfactant have recently allowed the growth of perfectly crystalline ultra-thin chemically disordered Fe–Cu alloy films in the whole composition range.[19] Today, some theoretical studies have also been performed on different over layer and surface alloys, e.g. Cu/Pb alloy deposited on Ru(0001),[20] Pt/Ru,[21] Pt/Au(111),[22] Al/Fe(100)[23] and Mn/Rh(100).[24]

In this work, the activity of crystalline single-layer substitutional Fe–Cu surface alloys in the initiation of the FTS process is hitherto considered by means of first-principles total energy calculations of the CO adsorption and dissociation processes. 25% and 50 %

* *Correspondence to:* *Elahifard, MohammadReza, Department of Engineering, Ardakan University, Ardakan, Iran, Email: mrelahifard@gmail.com

a *Department of Engineering, Ardakan University, Ardakan, Iran*

b *Department of Chemistry, Payame-Noor University, Tehran, Iran*

c *Medicinal Plants and Drugs Research Institute, Shahid Beheshti University, Tehran, Iran*

d *Department of Chemistry, Sharif University of Technology, Tehran, Iran*

substitutional impurities of Fe and Cu form the single-layer surface alloy structure on the (100) faces of *fcc*-Cu and *bcc*-Fe, respectively. On both elemental and alloy surfaces, the CO adsorption energy with ¼ ML CO as a catalytic activity index[25] is reported. Then, the CO adsorption energy of ½ ML and also CO dissociation barrier with ¼ ML CO were considered on the surface alloys. All calculations have been considered in two separate sections 1; alloys over *bcc*-Fe(100), and 2; alloys over *fcc*-Cu(100). We apply density functional theory (DFT) to our problem as it is presently the only applicable method, even though it is known[26] that none of the available functionals yields an overall correct description of CO–metal systems, with the simultaneously accurate description of adsorption site preference and metal properties being a notoriously hard problem.

Calculation method

Spin-density-functional theory total-energy calculations are carried out within the Projector-Augmented Waves (PAW) method as implemented in VASP.[27–30] The revised form of the Perdew, Burke and Ernzerhof (revPBE)[31,32] generalized-gradient approximation to the exchange-correlation energy functional is used throughout, for its accuracy in predicting adsorption energies as a rule of thumb. Although this is not related to a better description of the underlying physics,[26] it is the best choice in this work by focusing on the adsorption energy of initial, transition and final states.[33] A cut-off energy of 400 eV for the planewave expansion of the Kohn–Sham orbitals, using the RMM-DIIS algorithm,[34] a first-order Methfessel–Paxton smearing polynomial with 0.1 eV broadening width and Monkhorst–Pack k-point sampling meshes of 5×5×1 ((2×2) unit cell surface) and 15×15×15 (bulk) are used[35] in the calculation of the Fe(100), Cu (100) and the alloys over them-(2×2)–CO adsorption system.

The surfaces are modeled by a five-layer slab with 12 A° vacuum size, using a three-dimensional periodic super-cell approach with a (2×2) two-dimensional unit cell. All layers are allowed to relax with a force convergence criterion of 0.01 eV/A°. The resulting revPBE *bcc*-Fe and *fcc*-Cu equilibrium lattice constants are 2.855 and 3.70 A°, respectively, in agreement with experiment (2.87 and 3.615 A°) [36,37] and also, with previous theoretical work by 2.83 and 3.685 A°.[10,38] With these parameters, we obtain a local magnetic moment 2.20 μ_B for ferromagnetic *bcc*-Fe. The results agree very well with previous PAW-GGA calculations and experiment by 2.20 and 2.22 μ_B.[39]

A transition-state search algorithm based on the climbing-image nudged elastic band approach (CI-NEB)[40] followed by transition-state structure refinement is applied to the computation of reaction barriers. The highest energy image out of the CI-NEB calculation refines by performing a geometry optimization calculation as described above.

Results and discussion

One-layer surface alloys over *bcc*-Fe(100)

CO adsorption energy with ¼ ML

Bare Fe(100) surface. Fe(100) surface is the second most stable surface of *bcc*-Fe, after Fe(110), but is more reactive for FTS and more open. The most stable adsorption configuration of CO on Fe(100) is tilted by 42° on the fourfold hollow site (Fig. 1a), with an adsorption energy of 1.53 eV that is compare to the corresponding previous theoretical data with 1.5 eV and 42° as adsorption energy and angle of CO arrangement[10] and by 1.26 eV respect to the experimental data.[23] Also, tilting angels between 35° and 57° from the surface normal were reported using X-ray photoelectron diffraction [41] and near edge X-ray absorption fine structure.[42] The top site exhibits less reactivity, with an adsorption energy of 1.03 eV (Fig. 1a). The adsorption energy ($E_{ads.}$) calculated as below equation:

$$E_{ads.} = E_{(molecule+salb)} - E_{(slab)} - E_{(molecule)},$$

where $E_{(molecule+salb)}$ is the energy of adsorbate pulse slab system, $E_{(slab)}$ is the energy of the clean slab, and $E_{(molecule)}$ is the energy of isolated CO molecule in a cell with sides of 10 A°. Our result showed length of CO molecules by 1.14 A°, in agreement with previous result.[10]

Substitutional single-layer bcc-$Cu_{0.25}Fe_{0.75}$/Fe(100). On the basis of the ensemble effect, change the minimum space of an adsorption complex as an active site after alloy formation, the substitution of Fe atoms by Cu, the most stable adsorption site (4-fold) is expected to lead to a significant decrease in reactivity.

Figure 1b shows the CO adsorption energy on the local minima as stable sites considered. Similar to what happens on Fe(100), adsorption on the fourfold site leads by far (E_{ads}=1.21 eV) to the lowest energy state. As expected, the presence of substitutional copper on the fourfold hollow site, when bound by CO, has a lower adsorption energy, and, furthermore, a different orientation is adopted by adsorbed CO on this surface alloy. In this case, although the ensemble effect dominates, the ligand term has a positive contribution where the adsorption energy on the on-top site of Fe (upright, near form) is 0.02 eV more on this surface than on the bare Fe(100) surface, based on presence of two Cu atoms in the nearest neighbor of Fe atom, while on another on-top site of Fe that there are not any Cu atoms in the nearest neighbor, the adsorption energy is similar to bare Fe atom: 1.02 eV and 1.03 eV respectively. According to the ligand effect, increasing the number of inactive atoms in the nearest neighbor of active atom causes more reactivity (more adsorption energy) of the active atom.

Substitutional single-layer bcc-$Cu_{0.5}Fe_{0.5}$/Fe(100). There exist two options for the copper atoms to substitutionally sit on a single layer of the *bcc*-Fe(100)-p(2×2) surface unit cell, with 50% substitution: the nearest neighbor and the next-nearest neighbor configurations that the former is the most stable form, by 0.75 eV (Fig. 2). On the nearest neighbor surface, two Cu and two Fe atoms state as first neighbor of each Fe, while on another form four Cu atoms play that role, that shows the Fe–Fe interactions are stronger than the Fe–Cu interactions. The fourfold sites, which consist of two Cu atoms, have become unfavorable. Figure 1c contains the adsorption energies on the different sites. The on-top site provides the most stable configuration, with an adsorption energy of 1.05 eV that is higher than CO adsorption energy on on-top site of bare Fe(100) and $Cu_{0.25}Fe_{0.75}$/Fe(100) (far form) surfaces based on the ligand effect. Substitution of Fe atoms by Cu atoms decreases overall Fe atoms interaction causing the narrower d-band to increase the chemisorptions energy. In this case similar to $Cu_{0.25}Fe_{0.75}$/Fe(100) (near form) surface, there exist two Cu atoms in the nearest neighbor and also the same adsorption energy, resulting in the nearest atoms playing the main role in the ligand effect.

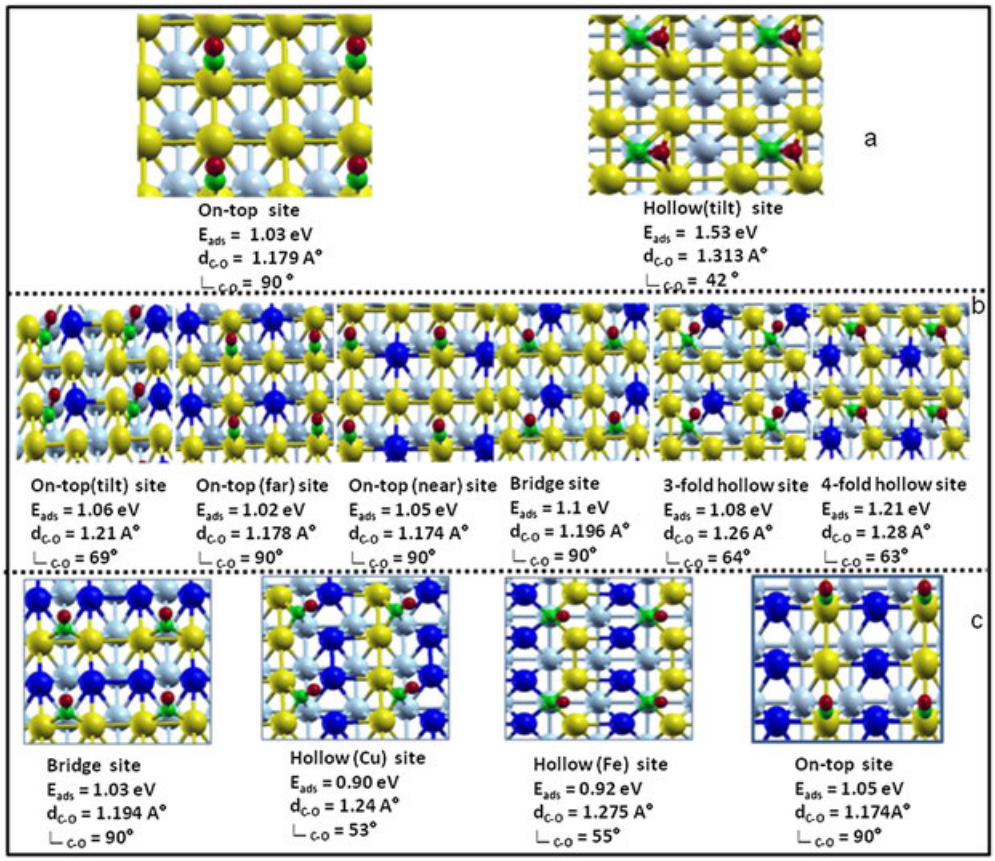

Figure 1. CO adsorption energy (1/4 ML) on the (a) bare *bcc*-Fe(100), (b) substitutional single-layer *bcc*-$Cu_{0.25}Fe_{0.75}$/Fe(100) and (c) single-layer substitutional *bcc*-$Cu_{0.5}Fe_{0.5}$/Fe(100). Blue, yellow, green and red spheres correspond to Cu, Fe, C and O atom, respectively. Light blue spheres represent the second layer, and $_{C\text{-}O}$ refers the angle between C–O bond and x–y surface.

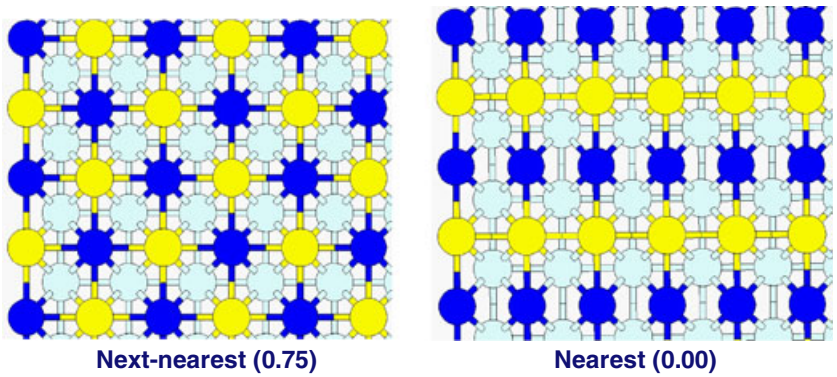

Figure 2. Relative energy of the two possible configurations for 50% Cu single-layer substitutional surface alloy on *bcc*-Fe(100): Next-nearest neighbor configuration and nearest neighbor configuration. Blue and yellow spheres correspond to Cu and Fe atoms, respectively. Light blue spheres represent the second layer.

Overall, as we expected, due to the fact that the fourfold site is the best site on the iron surface, the presence of Cu atoms destroys this site and creates a big ensemble effect leading to more weak strength of CO chemisorptions on the surface alloys.

CO adsorption with ½ ML

Previous result showed[10] that the CO adsorption energy with 50% CO coverage is 1.54 eV, while it is 1.50 eV with 25% CO coverage on Fe(100) surface. This referenced to the more capability of the surface to adsorb CO molecules with high regime that is a reason of the surface poisoning. Figure 3 shows the most stable configuration of ½ ML CO on the $Cu_{0.25}Fe_{0.75}$/Fe(100) and $Cu_{0.5}Fe_{0.5}$/Fe(100) surface alloys. Same as the bare Fe(100) surface, $Cu_{0.25}Fe_{0.75}$/Fe(100) surface alloy showed a light stronger adsorption (0.03 eV) with increasing the CO coverage from ¼ ML to ½ ML. However, in case of $Cu_{0.5}Fe_{0.5}$/Fe(100) surface alloy, our calculation results addressed the lower adsorption energy by 0.2 eV at ½ ML indicating the lower saturation coverage of this surface related to the bare Fe (100) and $Cu_{0.25}Fe_{0.75}$/Fe(100) surfaces.

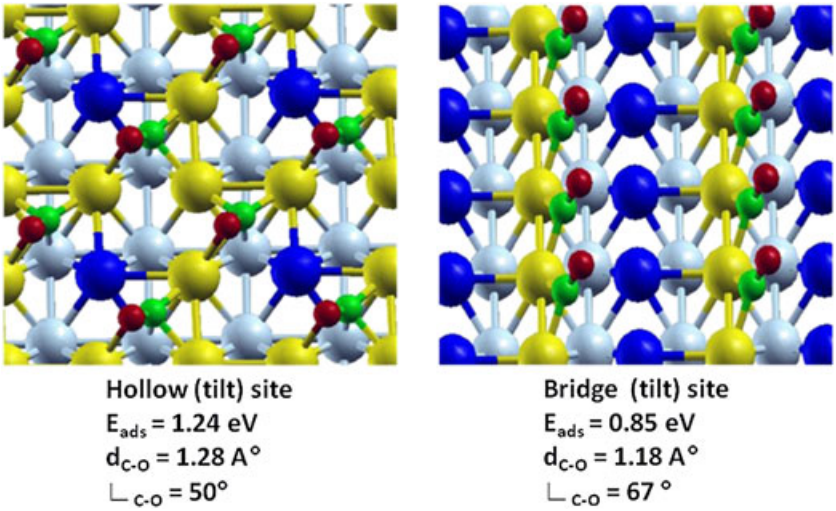

Figure 3. CO adsorption energy (1/2ML) on the substitutional single-layer *bcc*-$Cu_{0.25}Fe_{0.75}$/Fe(100) and single-layer substitutional *bcc*-$Cu_{0.5}Fe_{0.5}$/Fe(100). Blue, yellow, green and red spheres correspond to Cu, Fe, C and O atom, respectively. Light blue spheres represent the second layer.

CO dissociation on the $Cu_{0.25}Fe_{0.75}$/Fe(100) surface alloy over Fe(100)

Previous results showed the CO dissociation on the pure Fe(100) surface with barrier of 1.19 eV and reaction energy of −1.09 eV which includes diffusion of the oxygen atom away from the carbon to relieve repulsion.[10] The CO dissociation on the $Cu_{0.25}Fe_{0.75}$/Fe(100) showed (Fig. 4) the reaction energy of +0.02 eV firstly, final state given by the diffusion of the oxygen atom to the furthest hollow site with an overall energy of −0.78 eV. Although, it is an exothermic process overall, regarding to the activation energy for this process (1.62 eV) that is higher than adsorption energy, the direct CO dissociation is not possible on the $Cu_{0.25}Fe_{0.75}$/Fe(100) surface. It should be mentioned that too low activity of $Cu_{0.5}Fe_{0.5}$/Fe(100) surface alloy to CO adsorption causes directly CO dissociation process on this surface to be ignored.

One-layer surface alloy over *fcc*-Cu (100) surface

CO adsorption energy with ¼ ML

Pure Cu(100) surfaces. The Cu(100) as an inert surface to CO adsorption was considered as a support of Fe/Cu alloys in this work. In the low coverage regime (¼ ML), the on-top and the bridge sites are the best sites to CO adsorption (Fig. 5a) with 0.56 eV and 0.43 eV as adsorption energy, respectively, on the pure *fcc*-Cu(100) surface that is in agreement with previous experimental results by 0.53 eV [43], but showing a few distance *versus* previous theoretical result by 0.77 eV as adsorption energy.[44] Also, on-top site is experimentally seen as the preference site[45] on this surface.

Here, DFT results using revPBE functional reference the preference site correctly on pure Fe(100) and Cu(100) surfaces. But, this method is not overall confident as reported previously.[33] So, we cannot assert to the reliability of the calculated preference site of alloy surfaces. As a result, the preference site is hesitated whenever the

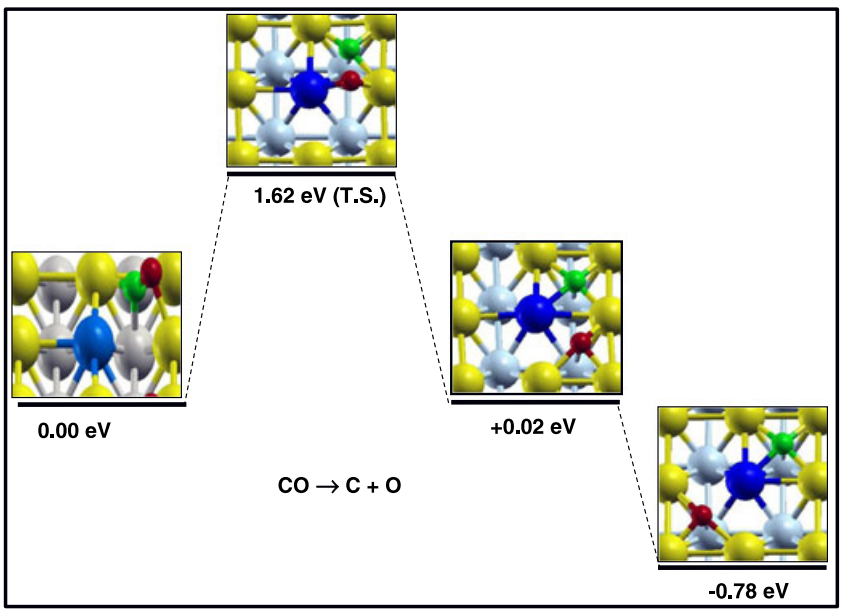

Figure 4. CO dissociation path (1/4ML) on the substitutional single-layer *bcc*-$Cu_{0.25}Fe_{0.75}$/Fe(100). Blue, yellow, green and red spheres correspond to Cu, Fe, C and O atom, respectively. Light blue spheres represent the second layer.

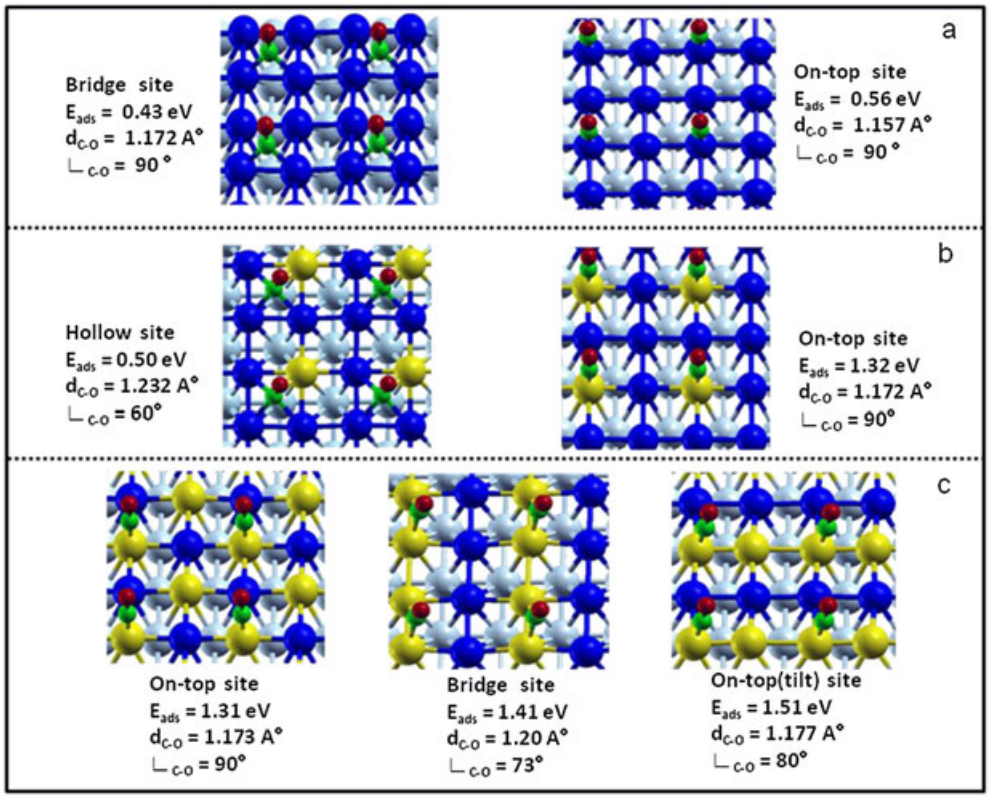

Figure 5. CO adsorption energy (1/4 ML) on the (a) bare *fcc*-Cu(100), (b) substitutional single-layer *fcc*- $Fe_{0.25}Cu_{0.75}$/Cu(100) and (c) substitutional single-layer $Fe_{0.5}Cu_{0.5}$/Cu(100). Blue, yellow, green and red spheres correspond to Cu, Fe, C and O atom, respectively. Light blue spheres represent the second layer.

small gap of adsorption energy (by 0.2 eV as the maximum absolute deviation of revPBE functional method[33]) presents between two or more stable sites; therefore, in that case, all of them should be considered for further studies.

The reason of this defect is not completely clear. It is proposed that the tendency of the DFT calculations to underestimate LUMO state of CO molecule causes the more overlapping of 2Π orbitals of CO with d-band of metal elucidating more magnitude of adsorption energy. In addition, since the degree of backdonating (2Π-metal interaction) increases with increasing coordination of CO in the adsorption site, i.e. hollow>bridge>on-top,[46] the wrongly relative adsorption energies are calculated on different sites. It means, as a DFT calculated preference site, the confidence to the on-top site is generally much more than to the hollow site.

Substitutional single-layer fcc-$Fe_{0.25}Cu_{0.75}$/Cu(100). It is expected that deposited Fe atoms surrounded with Cu atoms create the active sites with significant ligand effect on the surface alloys over the Cu(100).

The best site on the *fcc*-$Fe_{0.25}Cu_{0.75}$/Cu(100) surface is obviously the on-top site of Fe atoms (Fig. 5b). In this case, in addition to atoms on the bottom layers, four first and second nearest neighbors of every Fe atoms on the surfaces are Cu atoms; that also makes the semi-bare Fe atoms with a large ligand effect leading to the higher adsorption energy, i.e. the adsorption energy on the on-top site is ca 0.3 eV larger on this surface than on the pure and alloys-based Fe(100) surface. In terms of the Cu-supported alloy film, the hollow sites are not stable sites for CO adsorption as the same of pure Cu(100) surface.

Substitutional single-layer fcc-$Fe_{0.5}Cu_{0.5}$/Cu(100). The most stable form of $Fe_{0.5}Cu_{0.5}$ alloy over the *fcc*-Cu(100)-p(2×2) surface unit cell is the nearest form (similar to the same alloy on the Fe (100)) providing more Fe–Fe interaction, which creates the active bridge sites in addition to on-top site. The lower distance between atoms on the *fcc*-Cu(100) compared to the *bcc*-Fe(100) by 8% causes a lower gap between stability of two different states (nearest and next nearest) with 0.15 eV on the former one *versus* 0.75 eV for the latter one. Figure 5c shows the CO adsorption on different sites, which introduces the on-top sites as the best sites on the next-nearest and nearest alloy forms. Although a higher percentage of Fe atoms leads to lower ligand effect instead of $Fe_{0.25}Cu_{0.75}$ surface alloy, the tilted CO molecule to the Fe–Fe bridge site on the nearest alloy form increases the adsorption energy impressively with 1.51 eV. The tilted CO molecule on the bridge site as the second stable configuration shows a high adsorption energy with 1.41 eV, too.

To check the ligand effect in this surface solely, we consider the CO adsorption energy on the on-top site of Fe atom on the next-nearest alloy form (Fig. 5c) where four first nearest neighbors of Fe atoms are Cu atoms similar to $Fe_{0.25}Cu_{0.75}$ alloy case (Fig. 5b). Hence, according to the ligand effect, the same adsorption energy is estimated on these cases with light lower for the first one due to the presence of Fe atoms as the second neighbors, which are confirmed with our calculation, which showed the adsorption energy is equal to 1.31 eV and 1.32 eV for former and latter cases, respectively.

Therefore, in terms of alloys based on the *fcc*-Cu(100), the ligand effect plays the predominant effect leading to higher CO adsorption energy compared to the bare Fe(100) with the similar site (e.g. on-top site).

CO adsorption with ½ ML

Our calculation results showed the CO adsorption energy of 1.32 eV and 1.39 eV on the $Fe_{0.25}Cu_{0.75}$/Cu(100) and $Fe_{0.5}Cu_{0.5}$/Cu(100) surface, respectively, with ½ ML CO (Fig. 6). It shows that both surface alloys have less reactivity compared to Fe(100) surface, and in case of the latter one, the saturated coverage decreases impressively with different sites for CO molecules on the $Fe_{0.5}Cu_{0.5}$/Cu(100)-p(2×2) unit cell, i.e. tilt form on the on-top site and bridge site that may refer to more closed Fe–Fe atoms causing anti symmetrical adsorbed CO on this surface. However, on pure iron surfaces such as Fe(100), Fe(110) and Fe(310) and also $Fe_{0.25}Cu_{0.75}$/Cu(100) and $Cu_{0.25}Fe_{0.75}$/Fe(100) surface alloys, the adsorption energies of ¼ ML and ½ ML CO coverage are the same. High saturation coverage of the iron surfaces is an important factor in surface poisoning regretted on the $Fe_{0.5}Cu_{0.5}$/Cu(100) surface suggesting the ability of this surface to preserve more against poisoning. Also, in adverse of $Fe_{0.25}Cu_{0.75}$/Cu(100) surface alloy, it shows a high activity to CO adsorption at low coverage with 1.51 eV as adsorption energy around Fe(100) surface (1.53).

CO dissociation on the surface alloy over fcc-Cu(100)

In the final section to compare the activity of this surface with iron surfaces, we considered the reaction energy and barrier of CO dissociation on the $Fe_{0.5}Cu_{0.5}$/Cu(100) surfaces. Similar to iron surface, fourfold hollow sites are the best sites to O and C adsorption on the $Fe_{0.5}Cu_{0.5}$/Cu(100) surface. Our results showed that the CO dissociation on the $Fe_{0.25}Cu_{0.75}$/Cu(100) is too much endothermic reaction (+1.2) leading to impossibility of this process on this surface (Fig. 7). In case of $Fe_{0.5}Cu_{0.5}$/Cu(100) although, this process as net reaction thermodynamically has the high barrier (2.5eV) result in the direct CO dissociation may not occur that was represented by previous experimental work [47]. Hence, on this surface, the carbide site through direct CO dissociation is not possible on the catalyzed reaction.

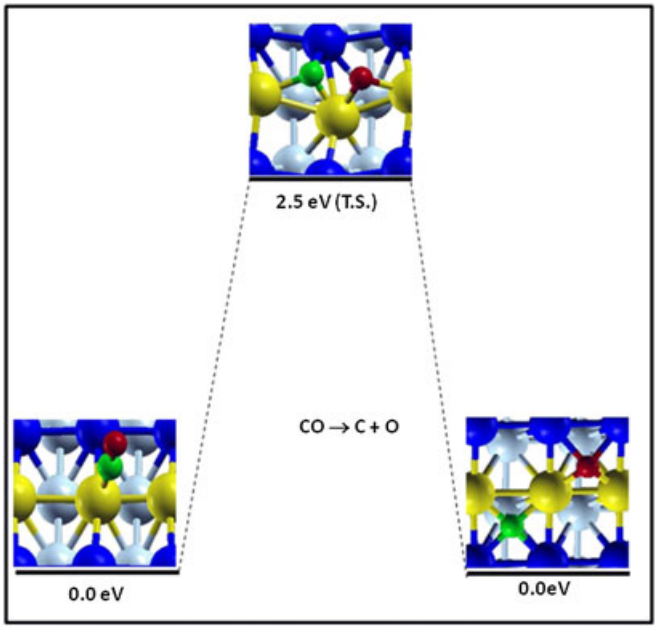

Figure 7. CO dissociation path (1/4ML) on the substitutional single-layer *fcc*-$Fe_{0.5}Cu_{0.5}$/Cu(100). Blue, yellow, green and red spheres correspond to Cu, Fe, C and O atom, respectively. Light blue spheres represent the second layer.

Conclusion

The CO adsorption behavior was studied on the single-layer substitutional Fe/Cu surface alloys over both *fcc*-Cu(100) and *bcc*-Fe(100) surfaces. Whereas the ensemble effect plays the dominant role for CO adsorption on the *bcc*-Fe(100) surface alloys (the most stable site disappears as a consequence of alloy formation), for the *fcc*-Cu(100) surface alloys, the ligand effect determines the CO stability. Our calculation results showed the first nearest neighbor atoms play major role in ligand effect. While $Cu_{0.5}Fe_{0.5}$/Fe(100) and $Fe_{0.25}Cu_{0.75}$/Cu(100) are inactive for CO dissociation, this process is possible thermodynamically on the $Cu_{0.25}Fe_{0.75}$/Fe(100) and $Fe_{0.5}Cu_{0.5}$/Cu(100), but it is not a possible reaction according to their barriers that are higher than their adsorption energies. Hence, it is proposed that direct dissociation cannot contribute to CO dissociation on these surfaces at catalysis reaction, and among all studied surfaces, only on the pure Fe(100) surface is the direct CO dissociation feasible.

Acknowledgement

The authors thank Prof. J.W. Niemantsverdriet for his stay at the Eindhoven University of Technology, during which this work was performed at the ST-HPC Cluster. Dr. M.Perez-Jigato is gratefully acknowledged for helping with this manuscript.

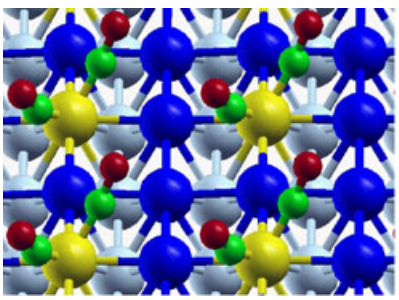

On-top (tilt) site
E_{ads} = 1.32 eV
d_{C-O} = 1.184 A°
$\angle_{C-O}$ = 61°

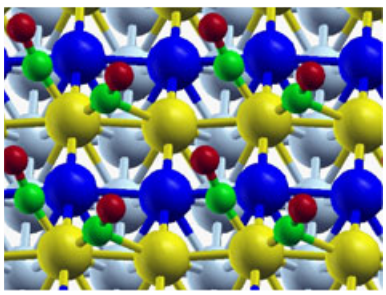

On-top (tilt)-bridge site
E_{ads} = 1.39 eV
d_{C-O} = 1.193-1.183 A°
$\angle_{C-O}$ = 60°-66°

Figure 6. CO adsorption energy (1/2 ML) on the substitutional single-layer *fcc*- $Fe_{0.25}Cu_{0.75}$/Cu(100) and substitutional single-layer *fcc*-$Fe_{0.5}Cu_{0.5}$/Cu(100). Blue, yellow, green and red spheres correspond to Cu, Fe, C and O atom, respectively. Light blue spheres represent the second layer.

REFERENCES

[1] J. M. H. Lo, T. Ziegler. *J. Phys. Chem. C* **2008**; *112*, 3679.
[2] G. Kresse, A. Gil, P. Sautet. *Phys. Rev. B* **2003**; *68*, 73401.
[3] P. Rochanaa, J. Wilcox. *Surf. Sci.* **2011**; *605*, 681.
[4] A. Groß. *Topics Catal.* **2006**; *37*, 29.
[5] A. Christensen, A. V. Ruban, P. Stoltze, K. W. Jacobsen, H. L. Skriver, J. K. Nørskov. *Phys. Rev. B* **1997**; *56*, 5822.
[6] E. Demirci, C. Carbogno, A. Groß, A. Winkler. *Phys. Rev. B* **2009**; *80*, 85421.
[7] A. Groß. *J. Phys.. Condens. Matter* **2009**; *21*, 84205.
[8] B. Hammer, J. K. Nørskov. *Surf. Sci.* **1995**; *343*, 211.
[9] I. Chorkendorff, J. W. Niemantsverdriet. Concepts of Modern Catalysis and Kinetics, (2nd edn)., Wiley, New York, **2007**.
[10] F. J. E. Scheijen, D. Curulla-Ferré, J. W. Niemantsverdriet. *J. Phys. Chem. C* **2009**;*113*, 11041.
[11] D. E. Jiang, E. A. Carter. *Surf. Sci.* **2004**; *570*, 167.
[12] M.R. Elahifard, M.P. Jigato, J.W. Niemantsverdriet. *ChemPhysChem* **2012**; *13*, 89.
[13] T. J. Vink, O. L. J. Gijzeman, J. W. Geus. *Surf. Sci.* **1985**; *150*, 14.
[14] O. L. J. Gijzeman, T. J. Vink, O. P. van Pruissen, J. W. Geus, J. Vac. *Sci. Technol. A* **1987**; *5*, 718.
[15] D. B. Bukur, D. Mukesh, S. A. Patel. *ind. Eng. Chem. Res.* **1990**; *29*, 194.
[16] P. Krüger. *Phys. Rev. B* **2001**; *64*, 94404.
[17] T. Bernhard, M. Baron, M. Gruyters, H. Winter. *Lett.* **2005**; *95*, 87601.
[18] H. Abe, K. Amemiya, D. Matsumura, J. Miyawaki, E. O. Sako, T. Ohtsuki, E. Sakai, T. Ohta. *Phys. Rev. B* **2008**; *77*, 54409.
[19] A. L. Barabási. *Fractal 1* **1993**; *846*.
[20] T. Hager, H. Rauscher, R. J. Behm. *Surf. Sci.* **2004**; *558*, 181.
[21] H. Hoster, B. Richter, R. J. Behm. *Phys. Chem. B*, **2004**; *108*, 14780.
[22] Y. Gohda, A. Groß. *J. Electroanal. Chem.* **2007**; *607*, 47.
[23] D. E. Jiang, A. E. Carter. *J. Phys. Chem. B* **2006**; *110*, 22213.
[24] F. Li, D.en Jiang, X. C. Zeng, Z. Chen. *Nanoscale* **2012**; *4*, 1123.
[25] J. K. Nørskov, T. Bligaard, A. Logadottir, S. Bahn, L. B. Hansen, M. Bollinger, H. Bengaard, B. Hammer, Z. Sljivancanin, M. Mavrikakis, Y. Xu, S. Dahl, C. J. H. Jacobsen. *J.Catal.* **2002**; *209*, 275.
[26] A. Stroppa, *G. Kresse. New J. Phys.* **2008**; *10*, 063020.
[27] G. Kresse, J. Furthmüller. *Comput. Mater. Sci.* **1996**; *6*, 15.
[28] G. Kresse, J. Hafner. *Phys. Rev. B* **1994**; *49*, 14251.
[29] P. E. Blöchl. *Phys. Rev. B* **1994**; *50*, 17953.
[30] G. Kresse, D. Joubert. *Phys. Rev. B* **1999**; *59*, 1758.
[31] J. P. Perdew, K. Burke, M. Ernzerhof. *Phys. Rev. Lett.* **1996**; *77*, 3865.
[32] B. Hammer, L. B. Hansen, J. K. Norskov. *Phys. Rev. B* **1999**; *59*, 7413.
[33] F. Abild-Pedersen, M. P. Andersson. *Surf. Sci.* **2007**; *601*, 1747.
[34] P. Pulay. *Chem. Phys. Lett*, **1980**; *73*, 393.
[35] H. J. Monkhorst, J. D. Pack. *Phys. Rev. B* **1976**; *13*, 5188.
[36] J. Sokolov, F. Jona, P. M. Marcus. *Phys. Rev. B* **1984**; *29*, 5402.
[37] W. T. Geng, M. Kim, A. J. Freeman. *Phys. Rev. B* **2001**; *63*, 245401.
[38] Z. Zuo, W. Huang, P. Han, Z. Li. *J. Mol. Model* **2009**; *15*, 1079.
[39] D. C. Sorescu. *J. Phys. Chem. C* **2008**; *112*, 10489.
[40] G. Henkelman, B. P. Uberuaga, H. Jónsson. *J. Chem. Phys.* **2000**; *113*, 9901.
[41] R. S. Saiki, G. S. Herman, M. Yamada, J. Osterwalder, C. S. Fadley. *Phys. Rev. Lett.* **1989**; *63*, 283.
[42] D. W. Moon, S. Cameron, F. Zaera, W. Eberhardt, R. Carr, S. L. Bernasek, J. L. Gland, D. J. Dwyer. *Surf. Sci. Lett.* **1987**; *180*, 123.
[43] S. Vollmer, G. Witte, C. Wöll. *Catalysis Letters* **2001**; *77*, 97.
[44] R. Marquardt, F. Cuvelier, R. A. Olsen, E. J. Baerends, J. C. Tremblay, P. Saalfrank. *J. Chem. Phys.* **2010**; *132*, 074108.
[45] S. Andersson, J. B. Pendry. *Phys. Rev. L* **1979**; *43*, 363.
[46] S. E. Mason, I. Grinberg, A. M. Rappe. *Phys. Rev. B* **2004**; *69*, 161401.
[47] O.L.J. Gijzeman, T. J. Vink, O.P. van Pruissen, J. W. Geus. *Sci. Technol. A* **1987**; *5*, 718.